An Innovative Organic Rankine Cycle System for Integrated Cooling and Heat Recovery

Angad Singh Panesar
School of Computing, Engineering and Mathematics, University of Brighton

Abstract

Converting a portion of the waste heat into usable power by implementing Rankine and Organic Rankine Cycles (ORC) on long-haul trucks is seen as a potential way to improve the overall system efficiency. To identify techno-economical heat sources across the drive cycle of a Heavy Duty Diesel Engine (HDDE), an energy and exergy analysis was performed on all the available heat streams. As a result, to recover the combined exhaust gases and coolant heat, a reference cascade system was analysed. Owing to the nature of this application, a size vs. performance optimisation was performed for the cascade system utilising water and R245fa fluid combination. Despite a 1.8% Brake Thermal Efficiency (BTE) improvement, the key consideration in the research and development efforts for ORC systems was identified as the investigation of technical paths that may improve the practicality of such a heat-to-power conversion concept. For this, simple holistic solutions were considered vital to meet the impending CO_2 regulations. To provide a potential solution, an innovative dual-pressure ORC system is therefore proposed to partially address the shortcomings of the cascade system. This innovative system is a function of new working fluids (i.e. water blends), its associated cycle operating mode and a novel architecture (i.e. direct engine block heat recovery). A screening and evaluation methodology applied to water-organic blends is presented. Simulations conducted in Aspen HYSYS V8 showed that, compared to the reference cascade system, the proposed dual-pressure system has the potential to deliver an average of 20% improvement in the system power, a 50% reduction in the total heat exchanger footprint, and a reduced system complexity. These advantages bode well for an integrated and relatively compact engine cooling and exhaust heat recovery solution for future automotive HDDEs. Implementation of the proposed system at mid-speed high-load engine operating condition increased the overall BTE from 41.4% to a maximum of 43.6%.

Keywords

Organic Rankine cycle; Diesel engines; Energy and exergy analysis; Size and performance trade-off; Water blends; Dual-pressure system

Nomenclature

A	heat transfer area (m^2)

E-mail address: A.Panesar@brighton.ac.uk
Tel: +44 (0)1273 642313

c_p	specific heat (kJ/kg°C)
$\dot{E}$	exergy (kW)
h	specific enthalpy (kJ/kg)
$\dot{I}$	irreversibility (kW)
$\dot{m}$	mass flow rate (kg/s)
M_{wt}	molecular weight (g/mol)
P	pressure (bar)
$\dot{Q}$	thermal duty (kW)
s	specific entropy (kJ/kg°C)
T	temperature (°C)
U	overall heat transfer coefficient (W/m^2°C)
$\dot{V}$	volume flow rate (m^3/s)
$\dot{W}$	power (kW)

Greek symbols

η	efficiency
ρ	density (kg/m^3)
Δ	difference

Abbreviations

B100	mid-speed high-load
B50	mid-speed mid-load
BTE	brake thermal efficiency
GWP	global warming potential
HDDE	heavy duty Diesel engine
HEX	heat exchanger
HP	high-pressure
HT	high-temperature
LP	low-pressure
LT	low-temperature
NFPA	National Fire Protection Association
ORC	organic Rankine cycle
PR	pressure ratio
SCR	selective catalytic reduction

UA product of heat transfer coefficient and area (W/°C)

VFR volume flow ratio

W28 28% water and 72% 1-propanol by mass

W47 47% water and 53% 3-ethyl-1-Butanol by mass

1 Introduction

The past decade has seen incremental improvements in automotive Heavy Duty Diesel Engine (HDDE) efficiency whilst complying with the exhaust emissions standards that have been the focus for engine developments [1]. The present crucial issue is the need for further engine efficiency improvements due to greenhouse emissions, impending fuel consumption regulations, increasing fuel costs and diminishing fossil fuel supplies. Key directions proposed by researchers and engine manufacturers to develop low carbon vehicles include: new engine architectures (e.g. extremely high compression ratio), powertrain efficiency enhancements (e.g. waste heat recovery) and use of alternative fuels (e.g. biodiesel) [2, 3]. The HDDE is expected to remain the prime mover of choice for long-haul trucks for the coming two decades due to its competitive efficiency, high power density, outstanding durability and drivability. Despite the efforts to directly increase the in-cylinder engine efficiency, a significant amount of the fuel energy is lost in the form of heat. As a result, heat-to-power conversion systems provide a good starting point and an attractive opportunity for emissions reduction whilst using a wasted resource.

There has been renewed interest in heat-to-power technologies in the automotive sector, with leading engine manufacturers, research centres and original equipment manufacturers announcing their research and development efforts over the decade [4, 5]. Various technologies have been proposed and are at the demonstration phase for converting a portion of the waste heat into either mechanical or electrical power. These include, but are not limited to, turbocompounding, thermoelectric generators and fluid bottoming cycles [6, 7]. Amongst the fluid bottoming cycle options, Organic Rankine Cycles (ORC) are being adopted as a premier technology for long-haul HDDEs when considering conversion efficiencies, technology readiness level, impending CO_2 legislations, absolute fuel consumption, base vehicle cost, space availability and weight penalty [8].

ORC systems with different complexity levels have been examined to target a variety of heat sources in the internal combustion engine. To recover the waste heat from the charge air, engine coolant and exhaust gases, Zhang et. al. analysed the characteristics of a dual-loop cascade system in combination with two conventional refrigerants (R245fa, R134a) for a light duty diesel engine [9]. In a similar dual-loop cascade system for a large scale engine, but excluding charge air, Song et. al. utilised water for the high temperature section, however in association with a screw expander for two-phase expansion [10]. While for exhaust heat recovery only, Shu et. al. selected alkanes owing to their excellent thermo-physical and environmental characteristics [11].

Adaptability of ORCs for different heat sources have led to the proposition of ORCs combined with other technologies. Shu et al. analysed a thermoelectric generator + ORC system to recover the coolant and exhaust heat [12], while, He et al. presented ORC + Kalina cycle system adding lubricant heat as the third heat source [13]. ORC systems have also been experimentally coupled to refrigeration and energy storage systems [14]. To address the mismatched demand and availability of energy, Pandiyarajan et. al. demonstrated the ability to store a noticeable level of fuel energy (10-15%) in the combined storage system, which was available at reasonably higher temperatures [15].

Important components like the expansion machines and heat exchangers are becoming more viable due to the synergies with the current automotive components and a series of crucial technological advancements. Both positive displacement expanders, in particular piston expanders, and dynamic machines, in particular radial turbines, have been suggested for automotive applications. Using simulation and experimental results, Seher et. al. showed two-stage turbine and piston expander mechanical efficiencies in the region of 65-85% [16]. In addition, Yang et. al. and Zhang et. al. have recently demonstrated prototypes of fin-tube and spiral-tube evaporators, respectively [17, 18]. As a result, on road demonstrations have shown that ORCs have the potential to improve the fuel economy of a long-haul truck by 6% [3]. The current market niche for ORCs is dependent on simplicity and affordability, with initial technology deployment on commercial vehicles expected during the middle of the next decade in the European Union and the United States.

This paper firstly presents an assessment of the various heat sources in an automotive HDDE for conversion into usable power. Secondly, the results of a cascade system to form a reference for comparison are presented as the consequence of the size vs. performance optimisation. Thirdly, the shortcomings of the cascade system utilising water and R245fa fluid combination are detailed for transport applications. For a comprehensive understanding, the system and performance parameters were based on the energy and exergy equations in all the specific points in the cycle. Finally, to partially address the shortcomings and facilitate the introduction of ORC systems, an innovative dual-pressure ORC system is proposed and examined extending the analysis of parallel works [19]. The primary objective functions for comparison between the reference system and the proposed system included system power, heat transfer footprint and size of the expansion machines. The simulations were conducted in an advanced chemical process modelling tool, Aspen HYSYS V8 [20].

2 Heat source assessment

The starting point of the study was the selection of a long-haul HDDE platform representative of the current and future productions, followed by the identification of realistic boundary conditions and assumptions for waste heat recovery analysis. As such, the simulation results of a 12.8-litre, 6-cylinder, single-stage turbocharged engine were utilised in this study [21]. Table 1 summarises the engine parameters at the mid-speed high-load condition (i.e. 1440 rpm and 100% power, denoted as B100) and the relevant input variables for the heat recovery analysis. The B100 engine operating condition was selected to perform a design study for the reference ORC system. The selected engine platform utilised a high efficiency Selective Catalytic Reduction (SCR) system as the only means to meet the Euro 6 oxides of nitrogen level. With a steadily increasing SCR efficiency, it is expected that exhaust gas recirculation may be phased-out by the end of the decade [3]. This will additionally offer marginal improvements in the base engine efficiency, and reduction in carbon deposits and engine wear [22, 23].

The selected HDDE platform offered exhaust gas, engine coolant, charge air and lubricant heat as the four potential sources of waste heat. Fig. 1a shows the fuel energy distribution at the B100 condition. The four sources collectively accounted for approximately 50% of the total fuel energy at the chosen speed-load point, and in fact, also over the entire engine operating range. Fig. 1a also shows 9.8% of the fuel energy termed as uneconomical exhaust. This is since, to give a true appreciation of the recoverable exhaust energy, the usable energy content was a function of the source temperature entering and leaving the specific heat exchanger. In case of the exhaust heat exchanger placed downstream of the aftertreatment devices, this was 420°C at inlet and limited to a minimum of 115°C at the outlet. The 115°C value then provided a small safety margin prior to the exhaust gases becoming susceptible to condensation. The exhaust gas composition (limited to N_2, CO_2, H_2O and O_2) was derived from the experimental results of a single-cylinder HDDE engine [19], resulting in a specific heat value of approximately 1.15 kJ/kg°C. In addition, exhaust lines were considered non-insulated and the exhaust temperature drop of 15°C over the aftertreatment devices was also included.

In order to account for variations in the waste heat temperatures, the four heat streams available in the heat exchangers were also assessed in terms of the exergy content [24]. The exergy content of a stream represents the maximum possible reversible work that can be extracted from a heat engine operating between the source and ambient temperature (assumed to be 25°C). Fig. 1b shows the energy and exergy content at B100 and the mid-speed mid-load condition (i.e. 1440 rpm and 50% power, denoted as B50). Charge air cooler heat and the lubricant heat due to low energy and exergy contents were excluded from heat recovery considerations. Charge air heat could only be considered at high load operation, but the efficient and dynamic cooling of this stream over the complete drive cycle may be a challenge. Lubricant heat, due to piston cooling, was typically 25% of the engine coolant heat, but due to the low quality (≈ 90°C) showed no noticeable benefit. As a result, only heat in the exhaust heat exchanger and the engine coolant heat were considered for conversion into power. Note that, conventional HDDEs are designed to operate with a mean engine coolant temperature of 90°C. To increase the coolant exergy content, raising the temperature level to a value of 115°C has also been suggested [25]. However, such a modification may result in increased NOx emissions, and additionally, increased urea consumption by the SCR system. Therefore, to assess the exergy content in this study, the coolant temperature was maintained at 90°C.

3 Reference cascade system

3.1 Rational for the reference

The availability of exhaust heat and engine coolant heat at two vastly different qualities but similar quantity levels is usually a challenge for the application of conventional single-loop ORC setups. This is principally due to the working fluid mass flow rate limitation, which either results in the underutilisation of the engine coolant heat, or liquid at the expansion machine inlet [19, 26]. Cascade systems which utilise independent heat recovery systems to match the specific source characteristics provide a potential solution [9, 10]. As a result, cascade systems appear to be a preferred option for exploitation of exhaust and engine coolant heat in the published literature, offering an appropriate reference for comparison.

3.2 System overview

A cascade system consists of two different temperature level cycles. The two closed-loop cycles, the High-Temperature (HT) and the Low-Temperature (LT) cycles are interconnected at least by a common heat exchanger. The common heat exchanger termed ‘cascade condenser’ is effectively an internal heat exchanger for the system. The cascade condenser acts as a condenser for the HT cycle and as an evaporator for the LT cycle. Only the condenser of the LT cycle plays a role in dissipating the heat out of the cascade system. Due to the high temperature differential across the system, need to limit exergy destruction and design considerations, two distinct working fluids are used. A higher boiling point fluid is used in the HT cycle, while the LT cycle utilises a relatively lower boiling point fluid.

Fig. 2a presents the simplified schematic layout of the thermal and subsystem architecture for the considered cascade system. The HT cycle recovered the exhaust heat downstream of the aftertreatment devices. Whereas the LT cycle recovered the engine coolant heat and the cascade heat load in series. The published literature indicated the suitability of water for heat source temperatures over 400°C and R245fa for heat source temperatures below 250°C [27, 28]. Hence, water and R245fa were used in the HT and the LT cycles, respectively. The bypass lines for the two expansion machines with pressure reducing valves were excluded for simplicity. Furthermore, fluid storage tanks prior to the two pumps and exhaust flow bypass valve were also omitted.

Table 2 summarises the system modelling overview. The equations are presented in terms of universal state points and can be adapted for the specific components in the cascade system. Where, $\dot{Q}$ is the thermal duty (kW), $\dot{m}$ is the mass flow rate (kg/s), c_p is the specific heat (kJ/kg°C), T is the temperature (K), $\dot{I}$ is the irreversibilities (kW), s is the entropy (kJ/kg°C), h is the enthalpy (kJ/kg), $\dot{V}$ is the volume flow (m^3/s), ΔP is the pressure change (Pa) and $\dot{W}$ is the work done or absorbed (kW). Also summarised are the modelling assumptions corresponding to realistic component efficiencies, performances and pressure losses. Where, η is the isentropic efficiency and PR is the expansion pressure ratio. The analysis leading to the justification of some of these assumptions is presented in Section 3.3.

For a fixed condensing temperature and a fixed minimum pinch point temperature difference in the three heat exchangers, the cascade systems net power variation was primarily a function of the parametric study of the HT cycle. This was since the maximum coolant temperature in the LT cycle limited the maximum evaporation pressure of R245fa. As a result, Fig. 3 presents the behaviour of the cascade system with variation in the maximum system pressure imposed in the HT cycle up to a value of 25 bar. With increasing HT cycle pressure, the net power in the HT cycle increased (Fig. 3a). This was due to the rate of thermal efficiency increase in the HT cycle being higher than the reduction in the quantity of exhaust heat recovered. However, with increasing HT cycle pressure, the net power in the LT cycle decreased (Fig. 3b). This was since firstly, the thermal efficiency of the LT cycle was constant due to the fixed temperature limits in the LT cycle, and secondly since the heat input into the LT cycle reduced due to a reduction in the cascade condenser heat load. Due to a lower heat input into the system with increasing HT cycle pressure, the additional fan power consumption also decreased. Collectively, with increasing HT cycle pressure, the combined system thermal efficiency and power increased (Fig. 3c). However, the rate of system power improvement at higher pressures (above 15 bar) was limited.

3.3 Size vs. performance trade-off

In order to quantify the practical performance improvement potential using the cascade system, a size vs. performance trade-off study was conducted for the five major system components. These being, the size of the HT expansion machine, the exhaust heat exchanger, the coolant heat exchanger, the cascade condenser and the air condenser. As a first approximation, the following was considered as an indicator of relative size variation for the heat exchangers and the air condenser. It was assumed that the overall heat transfer coefficient (U, W/m^2°C) remained relatively unchanged for a particular fluid under a fixed process type. Therefore, UA (W/°C), i.e. overall heat transfer coefficient multiplied by the heat transfer area (A, m^2), was considered as an indicator for the relative heat transfer size. Similarly, the PR of the expansion machine was considered as an indicator of the relative expansion machine size for a particular fluid under a fixed process type.

Fig. 4a shows the influence of the PR in the HT cycle on the combined expander power. The maximum combined power was achieved at a high PR value of 30:1. However, such levels of PRs are beyond the reach of any efficient single-stage expansion machine. As a trade-off, the design point pressure ratio was reduced to ≈ 12:1. This was since the combined expander power improvement with PRs above this value was relatively insignificant to justify the added size and the associated costs.

Fig. 4b shows the influence of the exhaust heat exchanger UA value on the HT expander power. There was an inflection region beyond which the UA value increased for a negligible improvement in the HT expander power. This inflection region corresponded to a minimum pinch point temperature difference of ≈ 10°C. A similar pinch point value (≈ 8°C) was also observed when considering the size of the coolant heat exchanger and the cascade condenser on the LT expander power (Fig. 4c). Larger areas will lower the heat transfer irreversibilities, but have a negative impact on system packaging and cost. All the heat transfer elements were subdivided into 20 equal working fluid enthalpy change sections to minimise the numerical error in the UA value.

Finally, Fig. 4d shows the influence of the air condenser UA value on the LT expander power. To achieve a realistic size trade-off with this component, while also addressing the cooling demand for other components, is perhaps one of the most vital modelling assumptions. This is since the performance of any fluid bottoming cycle is very sensitive to the heat rejection limit. However, due to packaging and frontal area constraints in automotive applications, overly optimistic condensing temperatures cannot be considered as a norm. Furthermore, the rebound effect is acknowledged rarely in the literature, i.e. fuel improvements may encourage the consumption of other energy forms which partially offset the gains [29]. The two relevant parameters in the present application include, low ORC condensing temperature, which increase the cooling fan power consumption, and excessively large exhaust heat exchanger surface area, which introduce HDDE pumping losses. Assuming that the ambient air temperature increases by 10°C over the air-to-air charge air cooler, the cooling air temperature available for the cascade system was 35°C. Therefore by limiting the air in the engine bay to 55°C for long-haul HDDEs, the inflection region then corresponded to an average design condensing temperature of ≈ 65°C (Fig. 4d). Table 2 summarises the pressure ratio, the pinch point and the condensing temperature values selected for simulations to offer a suitable techno-economical trade-off.

3.4 Results and discussion

Utilising the findings of the trade-off study, Fig. 2b describes the T-S diagram for the design point cascade system using water and R245fa combination, while Table 3 details the key system and performance parameters to act as a reference for comparison in further analysis. Note that the LT cycle was also the Low-Pressure (LP) cycle, and hence, the LT and LP notations were used interchangeably (this was also true for the HT cycle). The LT cycle recovered the cascade condensing load (Pt. 6 to 4) of the HT cycle to fully evaporate R245fa (Pt. 2 to 3), which underwent a slight superheated expansion (Pt. 3). Due to the low condensing pressure in the HT cycle, water was superheated to 250°C (Pt. 5) in order to maintain a dryness fraction of ≈ 1 (Pt. 6). Since the coolant heat exchanger was modelled with a pinch point of 8°C, the evaporating temperature of the LT cycle was fixed at 80°C (Refer to Fig. 2c for a zoomed in view of the LT section). This resulted in a PR and Volume Flow Ratio (VFR) of 1.3:1 and 1.4:1 for R245fa, making it suited to scroll and screw expanders [30]. The VFR seen in the HT cycle was also favourable at 8.6:1, and was within the reach of single-stage piston expanders [31]. The above mentioned positive displacement expanders have also shown successful operation with dryness fraction ≥ 0.90 [7].

The cascade system offered relatively lower maximum (10.9 bar) and minimum (0.6 bar) cycle pressures for both the temperature level cycles. The cascade cycle generated 13.5 kW of system power, increasing the overall engine BTE by 4.3%. The system power included the parasitic pump (0.6 kW) and fan power consumption (1.8 kW), along with the transmission losses (1.4 kW) for expanders and pumps. The expander (65%) and pump (55%) isentropic efficiencies were assumed to be constant. Although these efficiencies are functions of the fluid properties and application conditions, nonetheless as a first approximation, the considered values may provide an insight into the achievable performance. The system power also accounted for the base engine performance loss due to an increased backpressure. A net reduction of 1.6 kW in engine crankshaft power was calculated when an additional backpressure of 0.1 bar was introduced in the exhaust line. The exhaust heat exchanger is a potential source of inefficiency at high loads, and this has to be considered during process integration. Such levels of reductions are similar to those reported experimentally by Hossain and Bari [32]. It is important to highlight that, some simulation studies have shown an insignificant impact on the base engine due to the thermal physics associated with the cooling of exhaust gas stream when utilising a well-designed heat exchanger [33, 34]. However, for more realistic cases, where the derivatives of current production components are used with the low exhaust gas quality, a reduction in the crankshaft power is more likely. The properties of exhaust, coolant, water and R245fa were calculated using the Peng-Robinson property package [35].

4 Problem definition for the cascade system

4.1 Fluid focused

The specific use of R245fa and water as working fluids are not without their challenges. R245fa presents vastly dissimilar thermodynamic and thermo-physical properties when compared to the conventional engine coolant (50% ethylene-glycol, 50% water). As a result, the engine coolant loop cannot be replaced, and an additional coolant heat exchanger is suggested in the literature. Furthermore, R245fa has a high Global Warming Potential (GWP) of 1030 (relative to CO_2 for an integration time horizon of 100 years) [36]. Implementation of the recent mobile air-conditioning directive led to the banning of R134a (GWP 1370), and such regulations in the future may also apply to ORC systems requiring the use of fluids with GWP less than 150 [37].

Although water offers a thermally stable, non-flammable and environmentally friendly solution, the drawbacks of using water include high freezing temperature, mass flow control challenge in small capacity transient systems and lower heat recovery at practical HDDE exhaust temperature levels [7, 27]. The large latent heat drawback of water, which limits its application to higher source temperatures using conventional expansion machines, is evident in Fig. 2b. Despite a small 10°C pinch point value, the exhaust stream was only cooled to 147°C, rather than ≈ 115°C, till which condensation of exhaust gases can be avoided.

4.2 System focused

Over a complete drive cycle, a cascade system has to ensure dry vapours prior to both the expanders and liquid prior to both the pumps. This may present a challenge in providing efficient combined heat recovery for maximum system power benefit. More importantly, the inclusion of the coolant heat exchanger and the cascade condenser contributed negatively to the system irreversibilities and the heat transfer areas. Despite the size vs. performance trade-off, these two components collectively contributed 17% towards the system irreversibilities (Fig. 5a). More noticeably, these two components collectively accounted for ≈ 50% of the total heat transfer area of the system (Fig. 5b). The irreversibility equations, represented in terms of universal state points in Table 2, were used for Fig. 5a. The numerical correlations described in Ref. [38] for calculating the heat transfer areas employing a generic pure counter-current heat exchanger were used for Fig. 5b. Additionally, at the design point, the heat input into the LT cycle was approximately twice that of the HT cycle, while the thermal efficiency was only around 1/5th (Table 3). Therefore, cascade systems may be better suited to stationary large-scale output capacity units (> 100 kW), where near ambient condensing temperatures are possible, improving the LT cycle performance.

5 Proposed dual-pressure system

5.1 Method overview

The lower efficiencies and higher investment costs associated with conventional energy conversion approaches, along with the challenges highlighted in the previous section explain why relatively less attention has been given to engine coolant as a heat source in automotive applications. As a result, such LT sources require innovative approaches in heat recovery and/or power generation. In view of Fig. 5a and 5b, formulation of unique working fluids was identified as one of the key methods which could translate to noticeable benefits. The aim was to formulate a fluid that could potentially replace the conventional engine coolant loop with the ORC working fluid, and also offer suitability at HDDE exhaust temperature levels.

The use of water blends was considered as an alternative avenue to meet the complex requirements for automotive applications. Since the resurgence of ORCs for HDDEs is relatively new, the present research on water blends was insufficient to ascertain suitable blends [39]. As a result, an investigation of water blends to provide desired properties and characteristics with varied water mass fraction was undertaken. The developed blend screening methodology, presented in Table 4, was applied to examine over 500 documented water blends [40]. Justifications for the screening parameters relevant to the present application are provided during the discussions in Section 5.2 and 5.3. As a result of this screening methodology, two miscible, non-reactive, water-alcohol blends were identified as suitable candidates. These being, 28% water and 72% 1-propanol by mass (hereafter referred to as W28), and 47% water and 53% 3-ethyl-1-Butanol by mass (hereafter referred to as W47). The key thermodynamic and thermo-physical properties of the pure organic fluids are presented in Table 5. Also included are the National Fire Protection Association (NFPA) rating on health hazard (classified from 0 to 4; 0 corresponding to minimal and 4 corresponding to severe). Both the suggested alcohols as blend constituents offer a health hazard level of 1, this is the lowest among pure organic fluids considered in ORCs [19].

5.2 System overview

To offer a more suitable heat-to-power conversion unit over the cascade system, while exploiting high grade exhaust heat with high cycle temperatures and recovering complete engine block heat, the thermal and subsystem architecture shown in Fig. 6a using the identified water blends and its associated cycle operating mode is proposed. Conceptually, such a system is an adaptation of the multiple pressure level, steam generator concept, used in coal power plants. The system consists of a dual-pressure level heat recovery architecture. Two pumps are utilised to generate the different subsystem pressure levels. While the expansion is either performed using two independent expansion machines or a dual-pressure expansion machine (i.e. with two different pressure level inlets and one exit). The

Low-Pressure (LP) loop is also the LT loop recovering the engine block heat directly. Similarly, the High-Pressure (HP) loop is also the HT loop recovering the exhaust heat.

The sub-cooled liquid (Pt. 1) was pumped by the LP pump to a pressure corresponding to evaporation at 95°C and was distributed into two streams. One stream was used to recover the engine block heat directly (Pt. 2), avoiding the use of a large coolant heat exchanger and offering slightly higher evaporating temperatures (95 vs. 80°C). Compared to the conventional engine coolant, the dual-pressure system resulted in a relatively higher ΔT across the engine block and a phase difference at the engine block exit (single-phase vs. two-phase). Such modifications although unconventional, have previously been experimentally demonstrated [5]. The use of homogenous positive azeotropic blends (Table 4, property 1), as in this case, contrary to the use of zeotropic blends, then attempts to minimise the temperature rise along the engine block. In addition, use of azeotropic blends allows the use of pure fluid design methods, reducing the design intensity of the dual-pressure system.

The second stream was raised to the highest cycle pressure by the HP pump. The high pressure stream was preheated, evaporated and superheated (Pt. 4) in the exhaust heat exchanger. The blends mass flow rate was controlled to maintain the maximum temperature of 250°C. This maximum selected blend temperature was below the critical temperature of the pure organic constituents. In the absence of reliable thermal decomposition data for the blends (Table 4, property 7), subcritical temperatures and absolute temperatures limited to 250°C may then avoid thermal decomposition [41]. In practice, for all water blends the flow rate has to be controlled precisely to prevent extreme temperature excursions (e.g. large superheating) and exposure lengths (e.g. heat build-up during impaired flow conditions). The HP HT vapour was then expanded in the HP expander. The superheated working fluid stream exiting the HP expander (Pt. 5) was subsequently mixed with the two-phase LP LT stream exiting the engine block. The mass flow rates in the two-loops were controlled to form a superheated vapour after mixing (Pt. 3). This stream was then injected into the LP expander. Although, the temperature exiting the HP expander was much higher than the stream exiting the engine block, the pressure was maintained equal. Therefore, the behaviour of the dual-pressure system was subjected to the parametric study of the HP loop. Fig. 7 presents the behaviour of the dual-pressure system with variation in the maximum system pressure up to 32 bar. With increasing system pressure, the exhaust heat recovery was higher and relatively constant compared to the cascade system (Fig. 3a), while the system thermal efficiency and the system power increased. The increased exhaust heat recovery by the water blend compared to the use of pure water was due to the reduced latent heat (Table 4, property 2).

5.3 Results and discussion

The dual-pressure system was simulated with the same UA value of the air condenser (10490 W/°C) and the exhaust heat exchanger (2120 W/°C) as that in the cascade system. Although this assumption is subjected to inaccuracy in relative system heat transfer size comparison, e.g. condensers giving ±20% variation in the overall heat transfer coefficients between low pressure steam and light hydrocarbons [42]. Nonetheless, the overall heat transfer coefficients for the fluids considered in this paper were in the order of, water > W47 ≈ W28 > R245fa. As a result, when numerical correlations described in Ref. [38] for calculating the heat transfer areas were employed using a generic pure counter-current heat exchanger, it was found that, the performance reduction in the exhaust heat exchanger when replacing water with the water blends was compensated by the performance improvement in the air condenser when using water blends instead of R245fa. In addition, the dual-pressure system was also simulated with the same PR for the HP expander (12:1) as that in the cascade system.

Fig. 6b describes the T-S diagram for the dual-pressure system using W28 with these constraints, while Table 3 details the key system and performance parameters for the constrained dual-pressure system using both the blends (Refer to Fig. 6c for a zoomed in view of the LT section). It can be noticed that compared to water which is a highly wetting fluid (Fig. 2b), the blends were only slightly wetting under the temperature range of application (Fig. 6b). This was due to the drying nature of the pure organic constituents in the water blend (Table 4, property 4). As a result, when the blends are expanded from the saturated vapour line with real isentropic expansion efficiencies, they result in high dryness fraction at the exit.

Due to different working fluids between the cascade system and the dual-pressure system, VFR, defined as the ratio between the volumetric flow rates at the expander outlet to inlet was considered as a first indicator of the relative size of the expansion machine. The variation in the VFR for the HP expander among water, W47 and W28 was relatively low (8.6:1-10.1:1). A relatively low VFR variation (1.4:1-1.8:1) in the LP expander was also seen among R245fa, W28 and W47. This suggested that the resulting size variation among the different HP and LP expanders will be minimal.

The maximum cycle pressure for W28 and W47 was 14.7 and 11.1 bar, respectively. Since the cascade system recovered lower exhaust heat (123 vs. 139-141 kW) and the cascade condenser internally transferred heat in the system, it offered slightly lower air condenser load (222 vs. 236 kW). As a result, for an equal air condenser size and additional fan power consumption (1.8 kW) the mean condensing temperature for the dual-pressure system was slightly higher (66 vs. 70°C).

The values presented in Table 3 then correspond to a first approximation for comparing the cascade and the dual-pressure system. The dual-pressure system offered an average of 20% improvement in system power. Since the dual-pressure system avoided the use of the coolant heat exchanger and the cascade condenser, it excluded the associated heat transfer losses and reduced the system heat transfer footprint by 50%. Such a system is also expected to be more suited over the much more complex thermoelectric generators + ORC and ORC + Kalina cycle systems [12, 13]. Implementation of the dual-pressure system using W28 offered a system power of 17 kW, increasing the overall engine BTE by 5.3% from 41.4 to 43.2%. The resulting modified fuel energy balance for the engine + the dual-pressure ORC system is presented in Fig. 8.

In addition, to assess the relative power densities of the two systems, the review conducted for ORCs (and refrigeration) systems for HDDE suggested a relative weight distribution as presented in equation 1 [19]. Note that, the fluid, valve, piping, control, tank etc. are expected to make up over 1/3rd of the total system weight. It was assumed that the power-to-weight ratio of the reference cascade system was 1. Therefore, when considering a 50% lower heat exchanger weight and a 20% higher power output, the power-to-weight ratio of the proposed dual-pressure system improved by 33%. A higher power density system bodes well for truck applications.

$$\begin{aligned} kW/kg_{ref} = {} & 0.22 Heatexchangers + 0.12 Condenser \\ & + 0.2 Expanders + 0.12 Pumps + 0.34 \end{aligned} \qquad (1)$$

It is important to highlight that similarity to engine coolant properties (Table 4, property 8) and high engine compatibility (Table 4, property 9) was a primary consideration, since design and material changes to the engine blocks are challenging. Table 6 presents the relative comparison of the seven key fluid properties between the conventional engine coolant and, W28, W47, R245fa and water for direct engine block heat recovery. Using engine coolant as a reference, it was noticed that water blends demonstrated a higher level of suitability [43]. When considering density multiplied by heat capacity, as a first approximation of the fluid's heat absorption capacity, the blends displayed a higher level of similarity than R245fa (0.84-0.9 vs. 0.52). This may present a favourable case for the opportunity of replacing the conventional engine cooling loop. The properties of the water blends were calculated using the Wilson property package [35].

Like ethylene-glycol, propyl-alcohols followed by amyl-alcohols also show good compatibility with common metals/alloys (e.g. aluminium, brass, carbon steel, copper, stainless steel), O-Ring materials (e.g. EPDM, kalrez, natural rubber, neoprene, viton) and thermoplastics (e.g. acetal, PEEK, polypropylene, PTFE, PVDF) [19]. In addition both the blends offer freezing temperatures below -30°C (Table 4, property 3) and GWP below 20 (Table 4, property 6). This makes these blends suitable for automotive applications from cold temperatures in North America, to potential future regulations in Europe requiring the use of low GWP fluids in automotive ORCs.

5.4 The next challenge for ORC systems

The key system and performance parameters presented in Table 3 for the water blends were constrained, and to a certain extent, some of them were non-optimised in nature. The exhaust heat exchanger for both the water blends could be considered near-optimum since they cooled the exhaust gases to 115-120°C, resulting in a pinch point of 25-30°C in the heat exchanger. Exhaust gas cooling below 115°C was considered uneconomical due to the reducing exergy content of the heat stream and heat exchanger considerations to avoid condensation of exhaust gases. However, the PR of 12:1 in the HP expander may be a variable constraining the dual-pressure system performance. This is best understood with reference to Fig. 9, which shows the effect of increasing the PR of the HP expander (assuming fixed 65% isentropic efficiency). The water blends continue to offer higher combined expander power, and additionally, with a marginally diverging trend compared to water up to an ultra-high pressure ratio of 20:1. As a result, the water blends will offer a more favourable trade-off at increased PRs. Hence, after the selection of a suitable working fluid, the selection of an appropriate expansion machine is the next most important step since the performance of a fluid bottoming cycle strongly correlates with that of the expansion and power transfer unit. In addition, Fig. 5a also indicates that approximately 1/5th of the system losses in the cascade system were due to the expanders. As a result, in automotive exhaust heat recovery applications, which correspond to high temperature differentials between the heat source and the heat sink, the requirement of high PR, cost-effective, low-capacity and efficient expanders remains a key challenge that has to be overcome in both the discussed systems.

6 Conclusion

A practical energy and exergy analysis considering the different waste heat sources on a modern automotive HDDE demonstrated the use of exhaust and coolant heat to be the most beneficial across a wide engine operating region. These two sources offer relatively similar quantity but dissimilar quality levels of heat, presenting a challenge for the application of simple single-loop ORCs. The use of cascade systems appears to be a preferred solution in the published literature, allowing exhaust heat recovery and complete coolant heat recovery. A size vs. performance trade-off study was conducted to optimise such a cascade system using water and R245fa combination for the HT and the LT heat recovery, respectively. However, the high heat input (226 vs. 123 kW) into the low thermal efficiency section of the system (1.8 vs. 11.5%), lower than desired exhaust heat recovery (123 vs. 141 kW), and the irreversible losses (17%) and size (50%) introduced collectively due to the coolant heat exchanger and the cascade condenser showed such systems to be non-optimal for automotive applications.

The identified path to address the shortcomings of the cascade system was to formulate water blends that could potentially replace the engine coolant loop, offering higher exergy input, and increased exhaust heat recovery, offering higher overall conversion efficiency. The blend screening methodology developed to screen over 500 water blends resulted in the selection of 28% water and 72% 1-propanol by mass, and 47% water and 53% 3-Methyl-1-Butanol by mass with suitable trade-offs amongst the desired fluid properties. These properties included, azeotropic behaviour, ultra-low freezing temperatures, near-isentropic fluid vapour curve, ultra-low GWP, high thermal stability, compatibility with engine construction materials and low boiling point. The proposed system is a function of these water blends, the limited superheated operating condition for the HP expander, the direct engine block heat recovery and the dual pressure architecture. The architectural advantages of the dual-pressure system can provide an integrated and relatively compact engine and waste heat recovery solution for future HDDE platforms. This is since the system provided complete cooling of the engine block and replacement of the engine cooling radiator to an ORC condenser. Furthermore, the engineering challenges that may arise due to the replacement of the engine coolant to the water blends are expected to be low due to the high similarity in the fluid properties. Compared to the conventional cascade system, the innovative dual-pressure system showed an average of 20% improvement in system power and a 50% reduction in the total heat transfer footprint. This increased the system power density by 33%. The implementation of the dual-pressure system resulted in a 5.3% improvement in the overall engine BTE.

This paper has attempted to include realistic component performances and a wide range of parasitic losses in the ORC system. However, the limitations of the work presented include, firstly, the absence of accurate heat exchanger size comparison by optimising the heat exchanger models, and secondly, the precise expansion efficiencies by using expander models. These two items remain a theme of focus for future works. Finally, the necessity of high PR (> 12:1), cost-effective, low-capacity (< 20 kW) and efficient expanders (> 65%) has been identified as a vital research direction.

Acknowledgements

The author would like to acknowledge the support of the Advanced Engineering Centre with respect to provision of software tools and proof-reading.

References

1. Ruhkamp, L., et al., Post 2014 HD diesel engine concepts – upcoming demands and innovative approaches, in 5th International MTZ Conference, November 23-24, Mannheim, Germany. 2010.
2. Miller, S.L., et al., Assessing the feasibility of increasing engine efficiency through extreme compression. International Journal of Engine Research, 2011. 12(3): p. 293-307.

3. Stanton, D.W., Systematic Development of Highly Efficient and Clean Engines to Meet Future Commercial Vehicle Greenhouse Gas Regulations. SAE Int. J. Engines, 2013. 6(3): p. 1395-1480.
4. Stobart, R. and R. Weerasinghe, Heat Recovery and Bottoming Cycles for SI and CI Engines - A Perspective. 2006, SAE International, 10.4271/2006-01-0662.
5. Endo, T., et al., Study on Maximizing Exergy in Automotive Engines. 2007, SAE International, 10.4271/2007-01-0257.
6. Saidur, R., et al., Technologies to recover exhaust heat from internal combustion engines. Renewable and Sustainable Energy Reviews, 2012. 16(8): p. 5649-5659.
7. Sprouse III, C. and C. Depcik, Review of organic Rankine cycles for internal combustion engine exhaust waste heat recovery. Applied Thermal Engineering, 2013. 51(1–2): p. 711-722.
8. Edwards, S., et al., Waste Heat Recovery: The Next Challenge for Commercial Vehicle Thermomanagement. SAE Int. J. Commer. Veh., 2012. 5(1): p. 395-406.
9. Zhang, H.G., E.H. Wang, and B.Y. Fan, A performance analysis of a novel system of a dual loop bottoming organic Rankine cycle (ORC) with a light-duty diesel engine. Applied Energy, 2013. 102: p. 1504-1513.
10. Song, J. and C.-w. Gu, Performance analysis of a dual-loop organic Rankine cycle (ORC) system with wet steam expansion for engine waste heat recovery. Applied Energy, 2015. 156: p. 280-289.
11. Shu, G., et al., Alkanes as working fluids for high-temperature exhaust heat recovery of diesel engine using organic Rankine cycle. Applied Energy, 2014. 119: p. 204-217.
12. Shu, G., et al., Parametric and exergetic analysis of waste heat recovery system based on thermoelectric generator and organic rankine cycle utilizing R123. Energy, 2012. 45(1): p. 806-816.
13. He, M., et al., A combined thermodynamic cycle used for waste heat recovery of internal combustion engine. Energy, 2011. 36(12): p. 6821-6829.
14. Yılmaz, A., Transcritical organic Rankine vapor compression refrigeration system for intercity bus air-conditioning using engine exhaust heat. Energy, 2015. 82: p. 1047-1056.
15. Pandiyarajan, V., et al., Experimental investigation on heat recovery from diesel engine exhaust using finned shell and tube heat exchanger and thermal storage system. Applied Energy, 2011. 88(1): p. 77-87.
16. Seher, D., et al., Waste Heat Recovery for Commercial Vehicles with a Rankine Process, in 21st Aachen Colloquium Automobile and Engine Technology, October 8-12, Aachen, Germany. 2012.
17. Zhang, Y.-Q., et al., Development and experimental study on organic Rankine cycle system with single-screw expander for waste heat recovery from exhaust of diesel engine. Energy, 2014. 77: p. 499-508.
18. Yang, F., et al., Parametric optimization and performance analysis of ORC (organic Rankine cycle) for diesel engine waste heat recovery with a fin-and-tube evaporator. Energy, 2015. 91: p. 128-141.

19. Panesar, A., Waste Heat Recovery Using Fluid Bottoming Cycles For Heavy Duty Diesel Engines. 2015, PhD. thesis. School of Computing, Engineering and Mathematics, University of Brighton, DOI: 10.13140/RG.2.1.4559.0248.

20. Aspen Technology Software, HYSYS version 8. 2015.

21. Ricardo Software, WAVE version 8.1. 2015.

22. Agarwal, D., S.K. Singh, and A.K. Agarwal, Effect of Exhaust Gas Recirculation (EGR) on performance, emissions, deposits and durability of a constant speed compression ignition engine. Applied Energy, 2011. 88(8): p. 2900-2907.

23. Zheng, M., G.T. Reader, and J.G. Hawley, Diesel engine exhaust gas recirculation-a review on advanced and novel concepts. Energy Conversion and Management, 2004. 45(6): p. 883-900.

24. Schuster, A., S. Karellas, and R. Aumann, Efficiency optimization potential in supercritical Organic Rankine Cycles. Energy, 2010. 35(2): p. 1033-1039.

25. Ringler, J., et al., Rankine Cycle for Waste Heat Recovery of IC Engines. SAE Int. J. Engines, 2009. 2(1): p. 67-76.

26. Vaja, I. and A. Gambarotta, Internal Combustion Engine (ICE) bottoming with Organic Rankine Cycles (ORCs). Energy, 2010. 35(2): p. 1084-1093.

27. Domingues, A., H. Santos, and M. Costa, Analysis of vehicle exhaust waste heat recovery potential using a Rankine cycle. Energy, 2013. 49(0): p. 71-85.

28. Hountalas, D.T., et al., Improvement of bottoming cycle efficiency and heat rejection for HD truck applications by utilization of EGR and CAC heat. Energy Conversion and Management, 2012. 53(1): p. 19-32.

29. Yue, C., D. Han, and W. Pu, Analysis of the integrated characteristics of the CPS (combined power system) of a bottoming organic Rankine cycle and a diesel engine. Energy, 2014. 72: p. 739-751.

30. Chang, J.-C., et al., Experimental study on low-temperature organic Rankine cycle utilizing scroll type expander. Applied Energy, 2015. 155: p. 150-159.

31. Latz, G., S. Andersson, and K. Munch, Selecting an Expansion Machine for Vehicle Waste-Heat Recovery Systems Based on the Rankine Cycle. 2013, SAE International, 10.4271/2013-01-0552.

32. Hossain, S.N. and S. Bari, Additional Power Generation from the Exhaust Gas of Diesel Engine by Bottoming Rankine Cycle. 2013, SAE International, 10.4271/2013-01-1639.

33. Hussain, Q.E. and D.R. Brigham. Organic Rankine Cycle For Waste Heat Recovery In A Hybrid Vehicle. in International Design Engineering Technical Conferences & Computers and Information in Engineering Conference, August 15-18, Montreal, Canada. 2010.

34. Katsanos, C., et al., Potentiality for Optimizing Operational Performance and Thermal Management of Diesel Truck Engine Rankine Cycle by Recovering Heat in EGR Cooler. 2010, SAE International, 10.4271/2010-01-0315.
35. Aspen HYSYS V8, Physical Property Methods. 2015.
36. Yang, M.-H. and R.-H. Yeh, Thermodynamic and economic performances optimization of an organic Rankine cycle system utilizing exhaust gas of a large marine diesel engine. Applied Energy, 2015. 149: p. 1-12.
37. European Parliament, Directive 2006/40/EC of the European Parliament relating to emissions from air conditioning systems in motor vehicles.
38. Aspen HYSYS V8, Unit Operations Guide. 2015.
39. Shu, G., et al., Study of mixtures based on hydrocarbons used in ORC (Organic Rankine Cycle) for engine waste heat recovery. Energy, 2014. 74: p. 428-438.
40. DDBST. Online Dortmund Data Bank Search. Accessed on 04.04.2015; Available from: www.ddbst.com/ddb-search.html.
41. Absalam-Gadzhievich, D.T. and B.A. Ramazanovich, Research of Thermal Stability of Water Mixtures of Aliphatic Alcohols. Journal of Materials Science and Engineering A 2 (12) 786-790, 2012.
42. Perry, R.H. and D.W. Green, Perry's Chemical Engineers' Handbook. 2007, McGraw-Hill, ISBN 0070498415.
43. Caterpillar, Application and installation guide: Cooling systems. 2011.

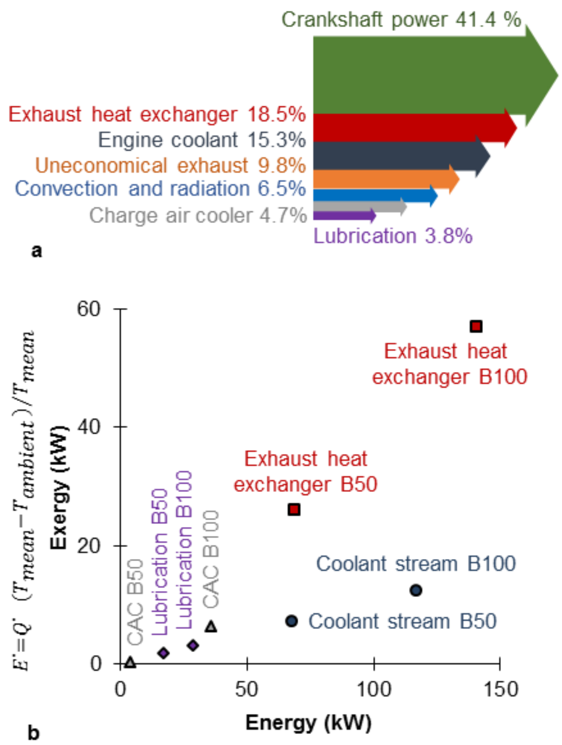

Figure 1 (a) Fuel energy distribution at B100 (b) Energy and exergy analysis of the heat sources at B50 and B100

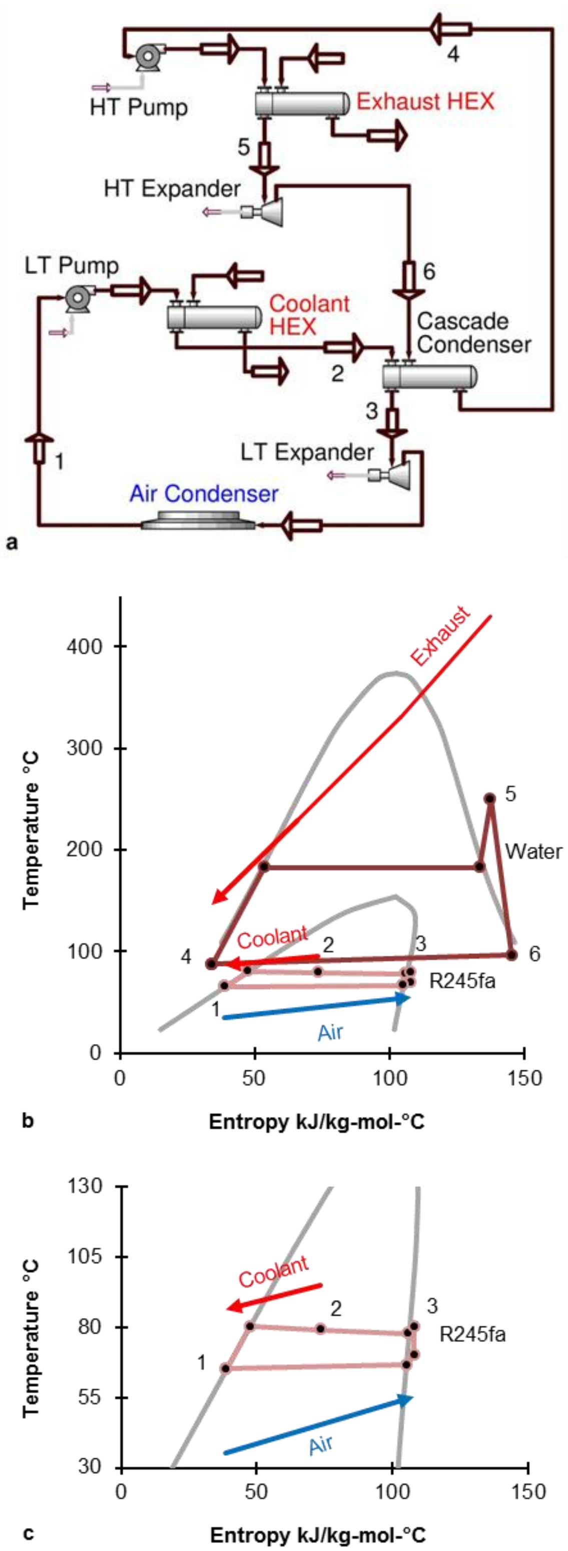

Figure 2 Cascade system (water, R245fa) (a) Schematic of the thermal and subsystem architecture, (b) T-S diagram at the system design point, and (c) Zoomed-in T-S diagram for the LT system section

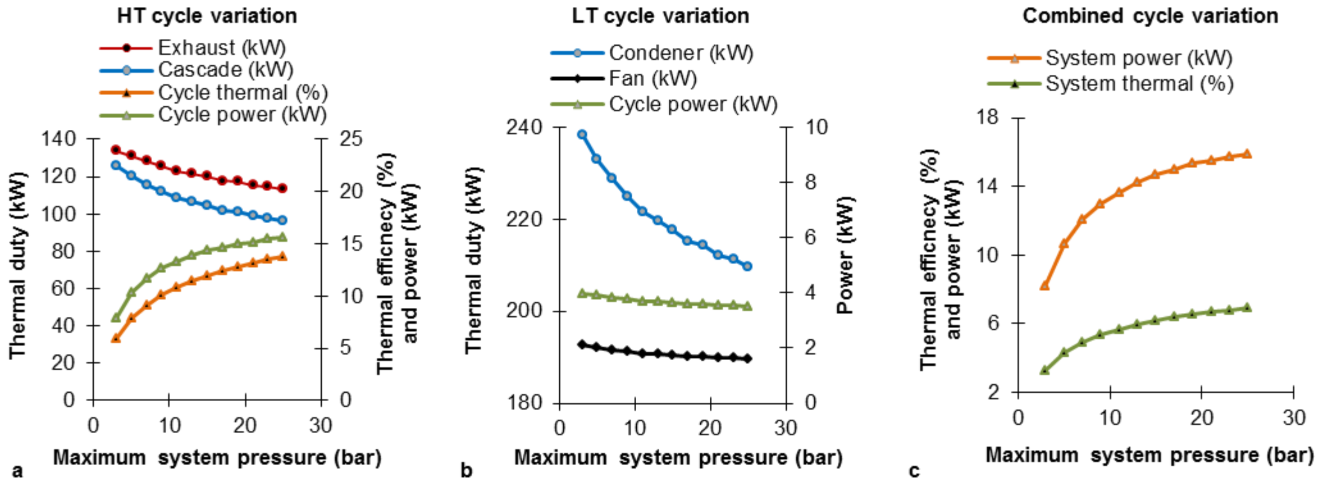

Figure 3 Effect of the maximum pressure in the cascade system (water, R245fa) (a) Variation in thermal loads, efficiency and power in the HT cycle (b) Variation in thermal load and power in the LT cycle, and (c) Variation in combined system power and system thermal efficiency

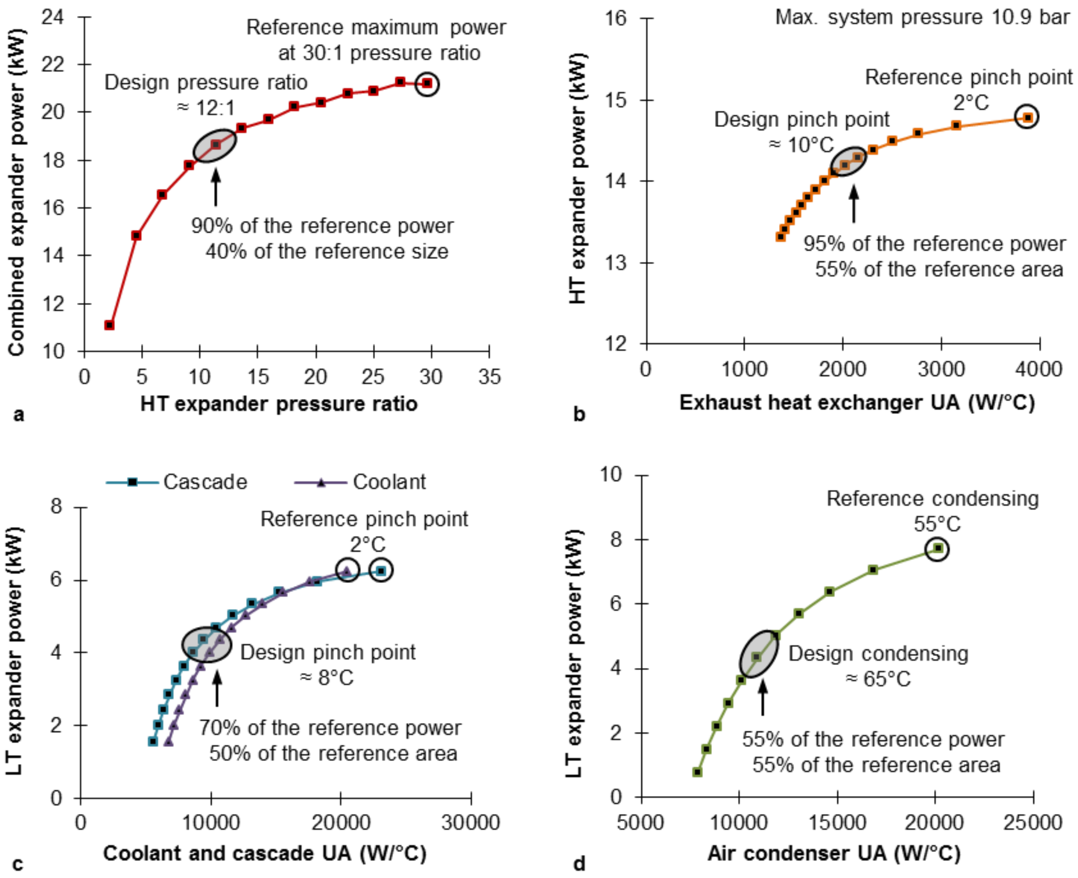

Figure 4 Equipment size vs. power produced trade-off for (a) HT expander (b) Exhaust heat exchanger (c) Coolant heat exchanger and cascade condenser, and (d) Air condenser

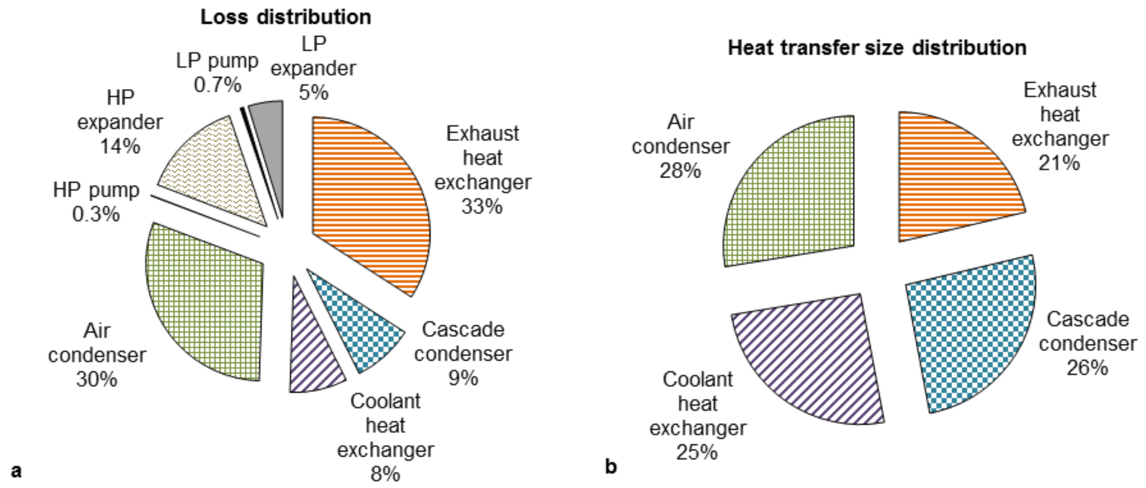

Figure 5 Cascade system (a) Relative irreversibility distribution by system components, and (b) Relative heat transfer size distribution by heat transfer elements

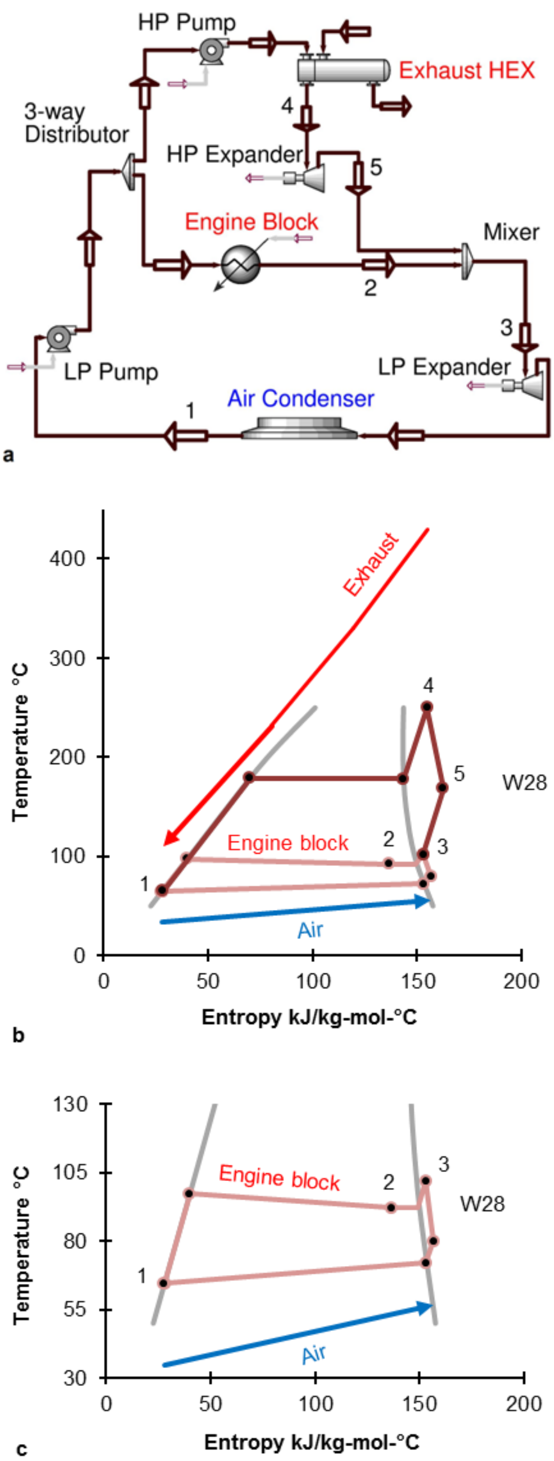

Figure 6 Dual-pressure system (a) Schematic of the thermal and subsystem architecture, (b) T-S diagram using W28 at the constrained point, and (c) Zoomed-in T-S diagram for the LT system section

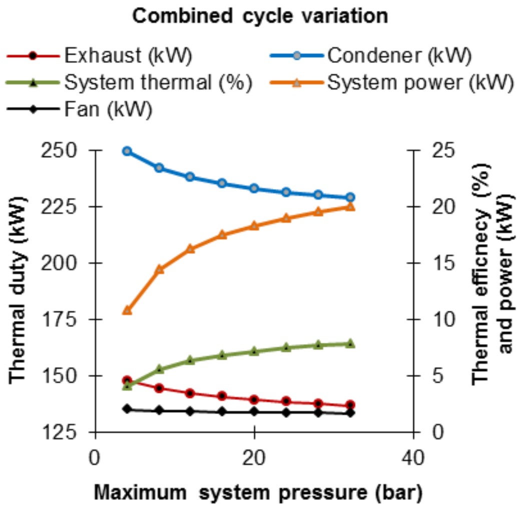

Figure 7 Effect of the maximum system pressure in the dual-pressure system on variation in thermal loads, system efficiency and system power using W28

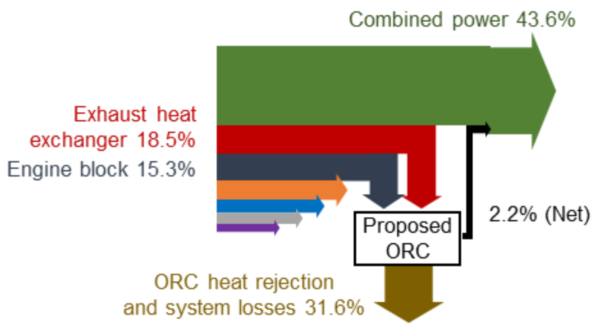

Figure 8 Fuel energy distribution at B100 for the engine combined with the dual-pressure ORC system

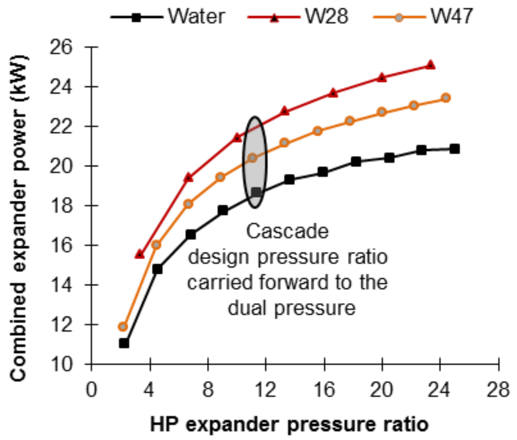

Figure 9 Advantage when using an efficient high PR piston expander in the dual-pressure system

Table 1 HDDE performance and the resulting variables for the heat recovery analysis

Variable	Value and unit
Air to fuel ratio	22.5:1
Speed	1440 rpm
$\dot{W}_{crankshaft}$	316 kW
$\eta_{brake\ thermal}$	41.4%
$T_{intake\ manifold}$	60°C
$P_{intake\ manifold}$	2.7 bar
$\dot{Q}_{coolant}$	117 kW (85-95°C)
$\dot{Q}_{charge\ air}$	36 kW (cooled from 150 to 60°C)
$\dot{Q}_{lubricant}$	27 kW (85-95°C)
$T_{cooling\ air\ inlet}$	35°C (secondary radiator)
$T_{cooling\ air\ exit}$	55°C
ΔP_{fan}	250 Pa
$\dot{W}_{fan}$	2 kW
$c_{p\ exhaust}$	1.15 kJ/kg°C
$\dot{m}_{exhaust}$	0.4 kg/s

Table 2 ORC energy and exergy modelling overview and equipment performance assumptions

Equipment	Modelling assumptions	Modelling overview
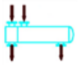	$\Delta P_{all\ heat\ transfer\ surfaces}$ = 0.25 bar $T_{minimum\ pinch\ point}$ = 8-10°C	$\dot{Q}_{heat\ exchanger} = \dot{m}_{source}\, c_{p\ source}\,(T_{inlet} - T_{exit})$ $\dot{I}_{heat\ exchanger} = T_{ambient}\,[\dot{m}_{fluid}\,(s_{exit} - s_{inlet}) + \dot{m}_{source}\,(s_{exit} - s_{inlet})]$
	η_{fan} = 65% $T_{minimum\ condesning}$ = 65°C	$\dot{I}_{air\ condenser} = T_{ambient}\,\dot{m}_{fluid}\,[(s_{exit} - s_{inlet}) - \{(h_{exit} - h_{inlet})/T_{mean}\}]$ $\dot{W}_{fan} = (\dot{V}_{air}\,\Delta P_{fan})/\eta_{fan\ and\ motor}$
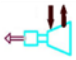	$\eta_{expander}$ = 65% $PR_{HP\ expander}$ = 12:1 $\eta_{all\ transmission}$ = 93% $T_{superheated}$ = 250°C	$\dot{W}_{expander} = \dot{m}_{fluid}\,(h_{inlet} - h_{exit\ ideal})\,\eta_{expander}$ $\dot{I}_{expander} = T_{ambient}\,\dot{m}_{fluid}\,(s_{exit} - s_{inlet})$
	η_{pump} = 55%	$\dot{W}_{pump} = \dot{m}_{fluid}\,(h_{exit\ ideal} - h_{inlet})/\eta_{pump}$ $\dot{I}_{pump} = T_{ambient}\,\dot{m}_{fluid}\,(s_{exit} - s_{inlet})$
		$\dot{\eta}_{system} = \dot{W}_{system}/\dot{Q}_{in}$ $\dot{W}_{system} = (\dot{W}_{HP\ exp} + \dot{W}_{LP\ exp} - \dot{W}_{HP\ pump} - \dot{W}_{LP\ pump})\,\eta_{transmission} - \dot{W}_{additional\ fan} - \dot{W}_{backpressure}$

Table 3 Key system and performance parameters for the cascade system and the dual-pressure system

		Cascade system Water, R245fa	Dual pressure system W28	Dual pressure system W47
$P_{system\ max}$	bar	10.9	14.7	11.1
$P_{system\ min}$	bar	0.6	0.4	0.3
$T_{system\ max}$	°C	250	250	250
$T_{system\ min}$	°C	65	64	63
$T_{evaporation}\ (HP)$	°C	183	178	173
$T_{condensation}\ (HP)$	°C	87	-	-
$PR_{expander}\ (HP)$		12:1	12:1	12:1
$VFR_{expander}\ (HP)$		8.6:1	10.1:1	9.9:1
$\dot{W}_{expander}\ (HP)$	kW	14.3	15.6	15.1
$\dot{W}_{pump}\ (HP)$	kW	0.1	0.3	0.2
$\dot{m}_{fluid}\ (HP)$	kg/s	0.05	0.09	0.08
$T_{evaporation}\ (LP)$	°C	80	95	95
$T_{condensation}\ (LP)$	°C	65	64	63
$P_{max}\ (LP)$	bar	7.9	1.5	1.2
$T_{max}\ (LP)$	°C	80	95	95
$PR_{expander}\ (LP)$		1.3:1	1.9:1	1.8:1
$VFR_{expander}\ (LP)$		1.4:1	1.8:1	1.7:1
$\dot{W}_{expander}\ (LP)$	kW	4.5	6.7	5.7
$\dot{W}_{pump}\ (LP)$	kW	0.5	0.1	0.1
$\dot{m}_{fluid}\ (LP)$	kg/s	1.29	0.11	0.09
$\dot{Q}_{exhaust\ heat\ exchanger}$	kW	123	141	139
$UA_{exhaust\ heat\ exchanger}$	W/°C	2120	2120	2120
$\dot{Q}_{cascade\ condenser}$	kW	109	-	-
$UA_{cascade\ condenser}$	W/°C	8630	-	-
$\dot{Q}_{coolant\ heat\ exchanger}$	kW	117	117	117
$UA_{coolant\ heat\ exchanger}$	W/°C	9900	-	-
$\dot{Q}_{air\ condenser}$	kW	222	236	236
$UA_{air\ condenser}$	W/°C	10490	10490	10490
$T_{air\ exit}$	°C	55	57	57
$\dot{m}_{cooling\ air}$	kg/s	10.95	10.95	10.95
$\dot{W}_{fan}$	kW	1.8	1.8	1.8
$\dot{W}_{backpressure}$	kW	1.6	1.6	1.6
η_{system}	%	5.6	6.6	6.1
$\dot{W}_{system}$	kW	13.5	17	15.7

Table 4 Screening methodology overview for the water-organic blend study

Number	Property	Value
1	Blend classification	Homogeneous positive azeotrope
2	Water mass fraction	25-50%
3	$T_{organic freezing}$	≤ −75°C
4	Number of atoms (organic)	10-20
5	Ozone depletion potential (organic)	0
6	Global warming potential (organic)	≤150
7	NFPA instability/reactivity rating (organic)	0 (minimal hazard)
8	Similarity to the engine coolant (blend)	High
9	Compatibility with engine materials (blend)	High
10	$T_{blend\ boiling}$	Lowest for a approximately similar water mass fraction

Table 5 Fluid properties for the chosen organic constituents

Formula	Name	$T_{critical}$ °C	$P_{critical}$ bar	$T_{boiling}$ °C	M_{wt} g/mol	ρ_{liquid} kg/m^3	$T_{freezing}$ °C	NFPA Health
$C_5H_{12}O$	3-Methyl-1-Butanol	304	39.3	131	88.1	812	-117	1
C_3H_8O	1-Propanol	264	51.7	97	60.1	806	-126	1

Table 6 Relative comparison of the key fluid properties for potential replacement of engine coolant at 90°C

	Engine coolant	W28	W47	R245fa	Water
Molecular weight, M_{wt}	1	1.30	1.12	4.80	0.65
Liquid density, ρ_{liquid}	1	0.80	0.85	1.14	0.97
Specific heat, c_p	1	1.05	1.06	0.46	1.31
Heat of vaporisation, H_{vap}	1	0.61	0.79	0.08	1.31
Surface tension, γ	1	0.75	0.93	0.20	0.50
Thermal conductivity, λ_{liquid}	1	0.48	0.51	0.18	1.96
Viscosity, $\mu_{dynamic}$	1	0.79	0.74	0.39	0.63